Full one-loop electroweak corrections to $h^0(H^0, A^0)H^{\pm}W^{\mp}$ associated productions at e^+e^- linear colliders

Liu Jing-Jing, Ma Wen-Gan, Zhang Ren-You, Guo Lei, Jiang Yi, and Han Liang

Department of Modern Physics, University of Science and Technology of China (USTC), Hefei, Anhui 230027, People's Republic of China

(Received 26 January 2007; published 22 March 2007)

We study the complete one-loop electroweak (EW) corrections to the processes of single charged Higgs boson production associated with a neutral Higgs boson (h^0, H^0, A^0) and a gauge boson $W^{\pm}$ in the framework of the minimal supersymmetric standard model (MSSM). Numerical results at the SPS1a′ benchmark point as proposed in the SPA project, are presented for demonstration. We find that for the process $e^+e^- \to h^0H^{\pm}W^{\mp}$ the EW relative correction can be either positive or negative and in the range of $-15\% \sim 20\%$ in our chosen parameter space. While for the processes $e^+e^- \to H^0(A^0)H^{\pm}W^{\mp}$ the corrections generally reduce the Born cross sections and the EW relative corrections are typically of order $-10\% \sim -20\%$.

DOI: 10.1103/PhysRevD.75.053007 PACS numbers: 12.15.Lk, 12.60.Jv, 14.70.Fm, 14.80.Cp

I. INTORDUCTION

Even though the standard model (SM) [1,2] has been successful in describing the strong, weak and electromagnetic interaction phenomena at the energy scale up to 10^2 GeV, it has been known for a long time that it is still considered as a low-energy effective theory suffering from a number of theoretical difficulties, such as hierarchy problem. It is likely that at the higher energy scale the minimal supersymmetric standard model (MSSM) [3–5] is the most attractive candidate among various extensions of the SM, which is expected to resolve theoretical difficulties existing in the SM. By adopting two Higgs doublets to preserve the supersymmetry in the MSSM, five Higgs bosons are predicted. They are two CP-even Higgs scalar bosons h^0 and H^0, one CP-odd Higgs boson A^0 and a charged Higgs pair $H^{\pm}$.

The charged Higgs boson plays an important role in the extensions of the SM as its discovery in experiment will unequivocally imply the existence of the physics beyond the SM. If the charged Higgs boson really exists in nature then it is mostly possible to be discovered in the coming few years at the CERN Large Hadron collider (LHC) due to its TeV scale colliding energy, but the further accurate measurements of masses of Higgs bosons and investigations of the properties of Higgs bosons [6], which is crucial for verification of electroweak (EW) symmetry breaking mechanism, need be best performed in a clean environment of e^+e^- collisions, such as at the future International Linear Collider (ILC) [7]. The study would be of the utmost importance for establishment of the MSSM or some of the more general supersymmetric models as the theory of the EW interactions. In addition, further study of the complete Higgs spectrum is the cornerstone of the definitive test of mechanism of electroweak symmetry breaking. In discovery and detailed study of the properties for these Higgs bosons, there are some important processes for neutral and charged Higgs bosons at linear colliders, such as, $e^+e^- \to Z^* \to h^0(H^0)Z^0$, $e^+e^- \to Z^* \to h^0(H^0)A^0$, $e^+e^- \to \nu\bar{\nu}W^{+*}W^{-*} \to \nu\bar{\nu}h^0(H^0)$, $e^+e^- \to H^+H^-$ and so on [8]. The lightest neutral Higgs boson h^0 in the MSSM has the mass upper limit of about 140 GeV, and it decays dominantly into $b\bar{b}$ pairs. For the heavier neutral Higgs bosons H^0/A^0, as a result of the strong enhancement of the coupling between Higgs boson and down-type fermions, both H^0 and A^0 will decay almost exclusively into $b\bar{b}$ ($\sim 90\%$) and $\tau^+\tau^-$ ($\sim 10\%$) pairs (The decays H^0, $A^0 \to t\bar{t}$ are possible only when they are kinematically allowed), and on the contrary all other decays are strongly suppressed [9–13]. For the mass of charged Higgs boson being blow 170 GeV–180 GeV (i.e., the $H^- \to \bar{t}b$ decay threshold), the dominant decay mode of the charged Higgs boson is $H^- \to \tau^-\bar{\nu}_\tau$. But when the mass of a charged Higgs boson is above the $H^- \to \bar{t}b$ decay threshold, the charged $H^{\pm}$ boson mainly decays into tb pair leading to $Wb\bar{b}$ final states [14].

If H^+H^- pair production at e^+e^- linear colliders (LC) is kinematically allowed, the dominant production process of charged Higgs bosons is the pair production via exchanging a virtual photon and Z boson $e^+e^- \to \gamma^*, Z^* \to H^+H^-$ [8]. For a fixed e^+e^- colliding energy, its cross section is related only with the charged Higgs boson mass. Another important production mode is the production of single charged Higgs boson, especially when the charged Higgs boson is too heavy to be produced in a pair at linear colliders. Among various single charged Higgs boson production channels, the bottom quark associated production process of $e^+e^- \to b\bar{b}H^{\pm}W^{\mp}$ [14] is experimentally interesting since it can be yielded by many topologies, such as the $t\bar{t}$ and H^+H^- pair productions followed by their corresponding sequential decays. The $e^+e^- \to b\bar{b}H^{\pm}W^{\mp}$ process can be also induced from following three single charged Higgs boson production processes (1) and the sequential decays $h^0(H^0, A^0) \to b\bar{b}$,

$$e^+e^- \to \Phi^0 H^\pm W^\mp, \qquad (\Phi^0 = h^0, H^0, A^0). \tag{1}$$

S. Kanemura, S. Moretti, *et al,* studied the processes of single charged Higgs boson production channels in the MSSM at LCs, including the processes (1) at tree-level in Ref. [14,15]. It was found that there are regions of parameter space where it is accessible beyond the kinematic limit for pair production, and these processes are excellent channels in studying the interactions among neutral Higgs boson (h^0, H^0 or A^0), charged Higgs boson and gauge boson ($W^\pm$), and is a useful alternative channel for studying the phenomenology of charged Higgs boson.

In present work, we will study the EW corrections to the processes (1) including complete one-loop diagrams in the MSSM. The paper is organized as follows: In Sec. II, we present the analytical calculation of the complete one-loop EW radiative corrections to $e^+e^- \to \Phi^0 H^\pm W^\mp (\Phi^0 = h^0, H^0, A^0)$ processes in the MSSM as well as the treatment of charged Higgs boson resonance. The numerical results and discussions are given in Sec. III. Finally, we give a short summary.

II. CALCULATIONS

A. Conventions and notations in analytical calculations

We denote the processes as

$$e^+(p_1) + e^-(p_2) \to \Phi^0(p_3) + H^+(p_4) + W^-(p_5), \qquad (\Phi^0 = h^0, H^0, A^0). \tag{2}$$

The lowest-order cross section reads

$$\sigma_{\text{tree}} = \frac{(2\pi)^4}{4|\vec{p}_1|\sqrt{s}} \int \bar{\sum_{\text{spin}}} |\mathcal{M}_{\text{tree}}|^2 d\Phi_3, \tag{3}$$

where $\vec{p}_1$ is the c.m.s. kinematical momentum of the incoming positron, The integration is performed over the three-body phase space of final particles $\Phi^0 H^+ W^-$, the bar over summation indicates averaging over initial spins. The phase-space element $d\Phi_3$ is defined by

$$d\Phi_3 = \delta^{(4)}\Big(p_1 + p_2 - \sum_{i=3}^{5} p_i\Big) \prod_{j=3}^{5} \frac{d^3\mathbf{p}_j}{(2\pi)^3 2E_j}. \tag{4}$$

In our calculation, we use dimensional reduction (DR) regularization scheme, which is supersymmetric invariant at least one-loop level, to regularize UV divergences and adopt on-shell (OS) conditions (neglecting the finite widths of the particle) to renormalize the relevant fields [16]. We adopt the 't Hooft-Feynman gauge and the definitions of one-loop integral functions in Ref. [17] in the calculation of one-loop diagrams. The Feynman diagrams and their corresponding amplitudes are created by *FeynArts* 3 [18] automatically, and the Feynman amplitudes are subsequently reduced by *FORM* [19]. We depict the lowest-order Feynman diagrams in Fig. 1. The numerical calculation of the two-, three- and four-point integral functions are done by using FF package [20]. The implementations of the scalar and the tensor five-point integrals are carried out exactly by using the Fortran programs as used in our previous works [21] with the approach presented in Ref. [22]. Because of the fact that the Yukawa coupling of Higgs/Goldstone to the fermions is proportional to the mass of the fermion, we ignore the contributions of the Feynman diagrams which involve the Yukawa coupling between any Higgs/Goldstone boson and electrons.

The $\mathcal{O}(\alpha_{\text{ew}})$ virtual correction to the cross section can be expressed as

$$\sigma_{\text{virtual}} = \sigma_{\text{tree}}\delta_{\text{virtual}} = \frac{(2\pi)^4}{2|\vec{p}_1|\sqrt{s}} \int d\Phi_3 \bar{\sum_{\text{spin}}} \text{Re}(\mathcal{M}_{\text{tree}}\mathcal{M}^\dagger_{\text{virtual}}), \tag{5}$$

where $\mathcal{M}_{\text{virtual}}$ is the renormalized amplitude involving all the one-loop electroweak Feynman diagrams and corresponding counter-terms [23].

The definitions and the explicit expressions of these renormalization constants can be found in Refs. [24–26]. Here we just list the definitions, which do not appear in Ref. [26], as below:

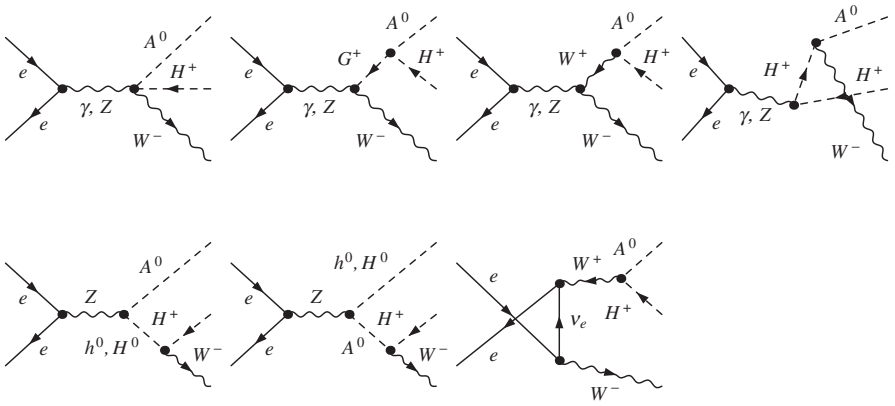

FIG. 1. The tree-level Feynman diagrams of the processes $e^+e^- \to \Phi^0 H^+ W^- (\Phi^0 = h^0, H^0, A^0)$.

$$\begin{pmatrix} G^{+(0)} \\ H^{+(0)} \end{pmatrix} = \begin{pmatrix} 1+\frac{1}{2}\delta Z_{G^+G^+} & \frac{1}{2}\delta Z_{G^+H^+} \\ \frac{1}{2}\delta Z_{H^+G^+} & 1+\frac{1}{2}\delta Z_{H^+H^+} \end{pmatrix} \begin{pmatrix} G^+ \\ H^+ \end{pmatrix},$$

$$\begin{aligned}
M^{(0)2}_{h^0} &= M^2_{h^0} + \delta M^2_{h^0}, \\
M^{(0)2}_{H^0} &= M^2_{H^0} + \delta M^2_{H^0}, \\
M^{(0)2}_{H^+} &= M^2_{H^+} + \delta M^2_{H^+}, \\
\delta M^2_{h^0} &= \widetilde{\mathrm{Re}}[\Sigma^{h^0h^0}(M^2_{h^0}) - b_{h^0h^0}], \\
\delta M^2_{H^0} &= \widetilde{\mathrm{Re}}[\Sigma^{H^0H^0}(M^2_{H^0}) - b_{H^0H^0}], \\
\delta M^2_{H^+} &= \widetilde{\mathrm{Re}}[\Sigma^{H^+H^+}(M^2_{H^+}) - b_{A^0A^0}], \\
\delta Z_{H^+H^+} &= -\widetilde{\mathrm{Re}}\frac{\partial \Sigma^{H^+H^+}(k^2)}{\partial k^2}\bigg|_{k^2=M^2_{H^+}}, \\
\delta Z_{G^+H^+} &= \frac{2}{M^2_{H^+}}\widetilde{\mathrm{Re}}[b_{G^0A^0} - \Sigma^{G^+H^+}(m^2_{H^+})], \\
\delta Z_{H^+G^+} &= -\frac{2}{M^2_{H^+}}\widetilde{\mathrm{Re}}[b_{G^0A^0} - \Sigma^{H^+G^+}(0)], \\
\delta Z_{G^+G^+} &= -\widetilde{\mathrm{Re}}\frac{\partial \Sigma^{G^+G^+}(k^2)}{\partial k^2}\bigg|_{k^2=0}.
\end{aligned} \tag{6}$$

The Higgs tadpole parameters $b_{A^0A^0}$, $b_{G^0A^0}$, $b_{h^0h^0}$, $b_{H^0h^0}$ and $b_{H^0H^0}$ are defined and expressed as in Ref. [25]. The operator $\widetilde{\mathrm{Re}}$ takes only the real part of the loop integrals and does not affect the possible complex couplings.

B. Disposal of the charged Higgs boson resonance

The disposal of H^- resonance in the calculation of the EW correction is similar with the method described in Ref. [27]. For the process $e^+e^- \to h^0H^+W^-$ in TeV scale colliding energy, the amplitude of the Feynman diagram with internal line of H^- [shown in Fig. 2(a), denoted as $\mathcal{M}^{H^-}_{\mathrm{tree}}(\Gamma_{H^-}=0)$) suffers from resonance effect when $s_{34} \equiv (p_3+p_4)^2 \to M^2_{H^-}$ due to the real charged Higgs boson decay $H^- \to h^0W^-$. We have to introduce the complex H^- mass to do the following replacement in the resonance propagator of the amplitude $\mathcal{M}^{H^-}_{\mathrm{tree}}(\Gamma_{H^-}=0)$,

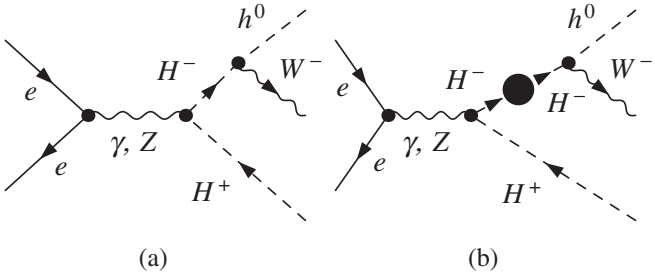

(a) (b)

FIG. 2. Feynman diagrams with charged Higgs boson resonance for process $e^+e^- \to h^0H^+W^-$.

$$\frac{1}{s_{34}-M^2_{H^-}} \to \frac{1}{s_{34}-M^2_{H^-}+i\mathcal{M}_{H^-}\Gamma_{H^-}}, \tag{7}$$

where Γ_{H^-} is H^- decay width. Then we get the amplitude at the tree-level as

$$\mathcal{M}^{H^-}_{\mathrm{tree}} = \frac{s_{34}-M^2_{H^-}}{s_{34}-M^2_{H^-}+i\mathcal{M}_{H^-}\Gamma_{H^-}}\mathcal{M}^{H^-}_{\mathrm{tree}}(\Gamma_{H^-}=0). \tag{8}$$

The modified amplitude $\mathcal{M}^{H^-}_{\mathrm{tree}}$ is a safe amplitude being free of the H^- resonance singularity. We know that at the tree-level calculation this replacement does not induce the gauge invariant and double-counting problems [27], but we should remember that after this treatment, there includes the contribution from the imaginary part of charged Higgs boson self-energy ($\Sigma^{H^-H^-}$) at higher order. In order to avoid the double-counting in calculation up to one-loop level, we should subtract the higher order contribution from the tree-level amplitude $\mathcal{M}^{H^-}_{\mathrm{tree}}$. In our practical calculation, we separate some special Feynman diagrams [shown in Fig. 2(b)] from entirety. Each of these diagrams in Fig. 2(b) contains a one-loop of charged Higgs boson self-energy, or the corresponding counterterm. Then we can express the one-loop level amplitude as below:

$$\begin{aligned}
\mathcal{M}^{\text{fix-width}}_{\text{one-loop}} = &[\mathcal{M}_{\text{one-loop}}(\Gamma_{H^-}=0) - \mathcal{M}_{H^-H^-\text{self}}(\Gamma_{H^-}=0)]_{(1/(S_{34}-M^2_{H^-}))\to(1/(S_{34}-M^2_{H^-}+iM_{H^-}\Gamma_{H^-}))} \\
&- \left[\frac{\Sigma^{H^-H^-}(s_{34}) - [\Sigma^{H^-H^-}(M^2_{H^-}) - b_{A^0A^0}]}{s_{34}-M^2_{H^-}} + \delta Z_{H^-H^-}\right]\mathcal{M}^{H^-}_{\mathrm{tree}},
\end{aligned} \tag{9}$$

where the first term on right-handed side is just the amplitude at one-loop level after subtracting the contributions of Fig. 2(b). The one-loop (or higher) order contributions are included by doing the replacement shown in Eq. (7). The real part of $\Sigma^{H^-H^-}(M^2_{H^-}) - b_{A^0A^0}$ is just equal to $\delta M^2_{H^-}$, the mass counterterm of charged Higgs boson, while $\Sigma^{H^-H^-}(M^2_{H^-}) - b_{A^0A^0}$ receives its imaginary part in the resonance from the subtraction of the $iM_{H^-}\Gamma_{H^-}$ contribution already contained in $\mathcal{M}^{H^-}_{\mathrm{tree}}$. In the calculation, charged Higgs boson width was evaluated using the HDECAY package [28], and UV divergence cancelled numerically.

C. Real photonic corrections

The $\mathcal{O}(\alpha_{\mathrm{ew}})$ virtual correction suffers from both ultraviolet (UV) and infrared (IR) divergences. It is checked numerically that the UV divergence vanished after renormalization. IR divergence comes from virtual photonic loop correction. It can be cancelled by the contribution of

the real photon emission processes. We denote the real photon emission as

$$e^+(p_1)+e^-(p_2)\rightarrow \Phi^0(p_3)+H^+(p_4)+W^-(p_5)+\gamma(k_\gamma),\quad (\Phi^0=h^0,H^0,A^0). \tag{10}$$

We adopt the general phase-space-slicing method [29] to separate the soft photon emission singularity from the real photon emission processes. By using this method, the bremsstrahlung phase space is divided into singular and nonsingular regions by the soft photon cutoff ΔE_γ, then the relative correction of the real photon emission is broken down into corresponding soft term $\delta_{\rm soft}$ with radiated photon energy $k_\gamma^0 < \Delta E_\gamma$ and hard terms $\delta_{\rm hard}$ with $k_\gamma^0 > \Delta E_\gamma$, where $k_\gamma^0=\sqrt{|\vec{k}_\gamma|^2+m_\gamma^2}$ and m_γ is the mass of photon, which is used to regulate the IR divergences existing in the soft term. The IR divergence from the soft contribution cancels that from the virtual correction exactly [30,31]. Therefore, the sum of the virtual and soft cross section is independent of the IR regulator m_γ. In the calculation, The phase-space integration of the processes $e^+e^-\rightarrow\Phi^0H^+W^-\gamma$, $(\Phi^0=h^0,H^0,A^0)$ with hard photon emission is performed by using the program *GRACE* [32]. The hard photon emission cross section $\sigma_{\rm hard}$ is UV and IR finite with $k_\gamma > \Delta E_\gamma$. Finally, we can get the UV and IR finite $\mathcal{O}(\alpha_{\rm ew})$ correction.

III. NUMERICAL RESULTS

In the numerical calculation, we use the following SM parameters [23]

$$\begin{aligned} m_e &= 0.510998902\ \text{MeV}, & m_\mu &= 105.658369\ \text{MeV},\\ m_\tau &= 1776.99\ \text{MeV}, & m_u &= 66\ \text{MeV},\\ m_c &= 1.2\ \text{GeV}, & m_t &= 178\ \text{GeV},\\ m_d &= 66\ \text{MeV}, & m_s &= 150\ \text{MeV},\\ m_b &= 4.7\ \text{GeV}, & m_W &= 80.425\ \text{GeV},\\ m_Z &= 91.1876\ \text{GeV}, & \alpha_{\rm ew}(0) &= 1/137.036. \end{aligned} \tag{11}$$

Here we take the effective values of the light quark masses (m_u and m_d) which can reproduce the hadronic contribution to the shift in the fine structure constant $\alpha_{\rm ew}(m_Z^2)$ [33]. As a numerical demonstration, we generally adopt the relevant supersymmetric parameters from the CP and R-parity invariant MSSM reference point SPS1a′ which is defined in the SPA project [34,35]. This point satisfies all the available high- and low-energy precision data and both the bounds for the masses of the SUSY particles and the bounds from cosmology. As we use the on-shell renormalization scheme, we have to transform the SPS1a′ $\overline{DR}$ input parameters $\mathcal{P}$ into on-shell parameters $\mathcal{P}^{\rm OS}$. This transformation is simply performed by subtracting the corresponding counter terms i. e. $\mathcal{P}^{\rm OS}=\mathcal{P}(Q)-\delta\mathcal{P}(Q)$. The input parameters for the reference point SPS1a′ are defined in the $\overline{DR}$ scheme at the scale $Q=1$ TeV, which are a set of mSUGRA parameters listed below:

$$M_{1/2}=250\ \text{GeV},\qquad M_0=70\ \text{GeV},\qquad A_0=-300\ \text{GeV}, \tag{12}$$

$$\text{sign}\,(\mu)=+1,\qquad \tan\beta(\tilde{M}=1\ \text{TeV})=10. \tag{13}$$

The relevant parameters of SPS1a′ point are listed in Table I.

Since the difference between $\overline{DR}$ and OS mass values for sparticle and Higgs bosons is of high order, either of them can be used. In our paper we generally adopt the $\overline{DR}$ masses of sparticle and Higgs boson, but when we study the cross sections as the functions of M_{A^0} or take $M_{A^0}\neq 424.9$ GeV, we still adopt the SPS1a′ MSSM spectrum and parameters except Higgs sector. In the later case the masses of the MSSM Higgs bosons are fixed by taking into account the significant radiative corrections in the MSSM by using FormCalc package with the input parameters: M_{A^0} and OS $\tan\beta$ value (i.e., $\tan\beta=10.31$ at SPS1a′ point) [36]. We checked in our calculation that the total cross section is independent on the IR regulator parameter m_γ and the soft cutoff δ_s. In following we take $m_\gamma=10^{-2}$ GeV and $\delta_s=10^{-4}$.

The Born and $\mathcal{O}(\alpha_{\rm ew})$ electroweak corrected cross sections at the SPS1a′ point for process $e^+e^-\rightarrow h^0H^+W^-$ as the functions of c.m.s energy in the energy range from 900 GeV to 1.8 TeV are illustrated in Fig. 3(a). The tree-level total cross section is drawn in a solid line, while the full one-loop EW corrected cross section is in a dashed line. We can read from the figure that at the position of $\sqrt{s}=1.3$ TeV, the Born and EW corrected cross sections are 0.019 fb and 0.015 fb, respectively. The corresponding relative corrections are depicted in Fig. 3(b) and we can see

TABLE I. Mass spectrum of supersymmetric particles and Higgs bosons in the reference point SPS1a′.

Particle	Mass (GeV)	Particle	Mass (GeV)
h^0	116.0	$\tilde{u}_R$	547.2
H^0	425.0	$\tilde{u}_L$	564.7
A^0	424.9	$\tilde{d}_R$	546.9
H^+	432.7	$\tilde{d}_R$	570.1
$\tilde{e}_R$	125.3	$\tilde{\tau}_1$	107.9
$\tilde{e}_L$	189.9	$\tilde{\tau}_2$	194.9
$\tilde{\nu}_e$	172.5	$\tilde{\nu}_\tau$	170.5
$\tilde{\chi}_1^0$	97.7	$\tilde{t}_1$	366.5
$\tilde{\chi}_2^0$	183.9	$\tilde{t}_2$	585.5
$\tilde{\chi}_3^0$	400.5	$\tilde{b}_1$	506.3
$\tilde{\chi}_4^0$	413.9	$\tilde{b}_2$	545.7
$\tilde{\chi}_1^+$	183.7		
$\tilde{\chi}_2^+$	415.4		

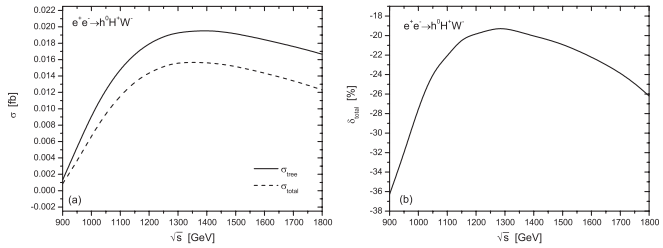

FIG. 3. The Born and full $\mathcal{O}(\alpha_{\rm ew})$ electroweak corrected cross sections as well as the corresponding relative corrections $\delta_{\rm total}$ as the functions of the c.m.s energy $\sqrt{s}$ at SPS1a′ point for process $e^+e^- \to h^0H^+W^-$. (a) cross section versus $\sqrt{s}$. (b) $\delta_{\rm total}$ versus $\sqrt{s}$.

that the absolute relative correction is very large when the colliding energy goes close to the vicinity of the threshold for process $e^+e^- \to h^0H^+W^-$. Figure 3(b) shows that when $\sqrt{s} = 900$ GeV, $\delta_{\rm total}$ is about -36%, but when the $\sqrt{s}$ goes to 1.3 TeV, the absolute relative correction declines to the value of 19.2%.

In Fig. 4(a), we present the Born cross section $\sigma_{\rm tree}$ and one-loop electroweak corrected cross section $\sigma_{\rm total}$ with $M_{A^0} = 200$ GeV and related MSSM parameters being taken from SPS1a′ scenario except Higgs sector for reaction $e^+e^- \to h^0H^+W^-$. In this case the mass of the lightest neutral Higgs boson M_{h^0} is equal to 117.2 GeV, which is fixed in the MSSM by using FormCalc program with the input parameters: $M_{A^0} = 200$ GeV and OS $\tan\beta = 10.31$. In contrast with the plots in Figs. 3(a) and 3(b), the complete EW one-loop corrections enhance Born cross sections as shown in Figs. 4(a) and 4(b), and both the $\sigma_{\rm tree}$ and the EW corrected $\sigma_{\rm total}$ in Fig. 4(a) are at least one order larger than in Fig. 3(a). $\sigma_{\rm total}$ can reach maximal value 0.33 fb at c.m.s energy near 700 GeV and decreases smoothly with the increment of $\sqrt{s}$. The corresponding relative correction is depicted in Fig. 4(b) in the same parameter space, the correction varies gently from 9% to 21.4%.

In Figs. 5(a) and 5(b) we depict the Born and EW corrected cross sections and corresponding relative corrections as the functions of mass M_{A^0} with $\sqrt{s} = 1000$ GeV and the relevant MSSM parameters adopting from the SPS1a′ point except Higgs sector for process $e^+e^- \to h^0H^+W^-$. The other Higgs boson masses are determined in the MSSM by using FormCalc program with M_{A^0} and OS $\tan\beta = 10.31$ being its input parameters. The values of M_{h^0} and M_{H^+} corresponding to different M_{A^0} values are also scaled on x-axes in Figs. 5(a) and 5(b). In Fig. 5(a), we see there is an abrupt change on each curve due to the resonance effect of $H^+ \to h^0W^+$ at the position around $M_{A^0} \sim 180$ GeV (where $M_{h^0} = 116.8$ GeV and $M_{H^+} = 197.2$ GeV). After reaching its maximal value at position of $M_{A^0} = 210$ GeV, the Born electroweak corrected cross sections decrease gently. The dependence of relative correction on M_{A^0} (or M_{h^0}, M_{H^+}) is displayed in Fig. 5(b). The $\delta_{\rm total}$ curve bends downward in the vicinity of $M_{A^0} \sim 180$ GeV because of resonance effect, and then decreases as M_{A^0} goes up. The relative correction varies from a positive to negative value region and the absolute value exceeds 10% for both light and heavy Higgs bosons.

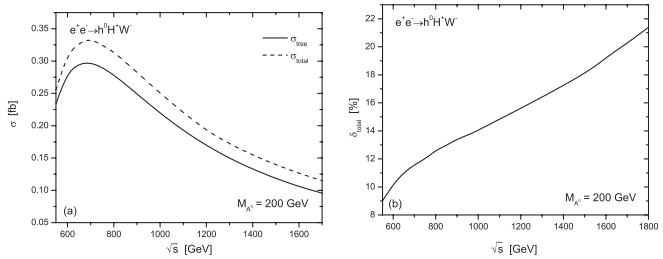

FIG. 4. The Born and full $\mathcal{O}(\alpha_{\rm ew})$ electroweak corrected cross sections as well as the corresponding relative corrections $\delta_{\rm total}$ as the functions of the c.m.s energy $\sqrt{s}$ with $M_{A^0} = 200$ GeV and related MSSM parameters being taken from the SPS1a′ scenario except Higgs sector for process $e^+e^- \to h^0H^+W^-$. (a) cross section versus $\sqrt{s}$, (b) $\delta_{\rm total}$ versus $\sqrt{s}$.

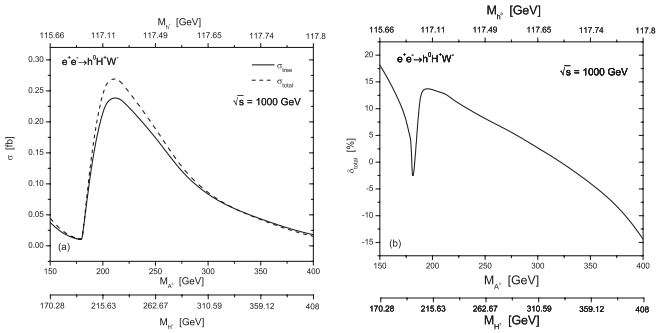

FIG. 5. The Born and full $\mathcal{O}(\alpha_{\rm ew})$ electroweak corrected cross sections as well as the corresponding EW relative corrections $\delta_{\rm total}$ as the functions of M_{A^0} with $\sqrt{s} = 1000$ GeV and relevant MSSM parameters taken from SPS1a′ point except Higgs sector being obtained by running FormCalc program with input parameters: M_{H^0} and OS $\tan\beta = 10.31$, for process $e^+e^- \to h^0H^+W^-$. (a) cross section versus M_{A^0}, (b) relative correction versus M_{A^0}.

We depict the Born and full one-loop electroweak corrected cross sections as the functions of c.m.s energy $\sqrt{s}$ with the MSSM parameters at the SPS1a′ point in Figs. 6(a) and 6(b) for process $e^+e^- \to H^0H^+W^-$ and $e^+e^- \to A^0H^+W^-$, separately. In the SPS1a′ scenario, the value of heavier neutral and charged Higgs boson masses (M_{H^0}, M_{A^0} and M_{H^+}) have the values beyond 420 GeV, accordingly the threshold energy of this parameter choice can reach 950 GeV. Therefore, in Figs. 6(a) and 6(b) we plot the c.m.s. energy $\sqrt{s}$ in the range between 1000 GeV and 1800 GeV. We see both of Born and $\mathcal{O}(\alpha_{\rm ew})$ corrected cross sections increase with the increment of the colliding energy. Figures 6(c) and 6(d) show the dependence of the relative corrections $\delta_{\rm total}$ of processes $e^+e^- \to H^0H^+W^-$ and $e^+e^- \to A^0H^+W^-$ on the c.m.s energy $\sqrt{s}$ respectively, with the same MSSM parameters

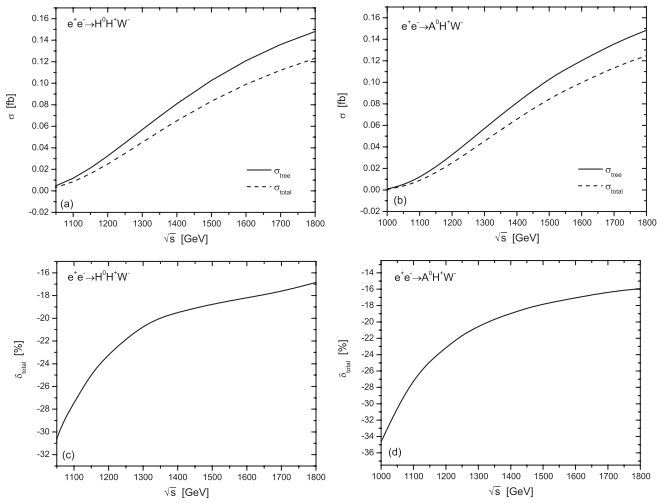

FIG. 6. The Born and full $\mathcal{O}(\alpha_{\rm ew})$ electroweak corrected cross sections as well as the corresponding relative corrections $\delta_{\rm total}$ as the functions of the c.m.s energy $\sqrt{s}$ in the SPS1a′ scenario for process $e^+e^- \to H^0(A^0)H^+W^-$. (a) cross section versus $\sqrt{s}$ for $e^+e^- \to H^0H^+W^-$, (b) cross section versus $\sqrt{s}$ for $e^+e^- \to A^0H^+W^-$, (c) $\delta_{\rm total}$ versus $\sqrt{s}$ for $e^+e^- \to H^0H^+W^-$, (d) $\delta_{\rm total}$ versus $\sqrt{s}$ for $e^+e^- \to A^0H^+W^-$.

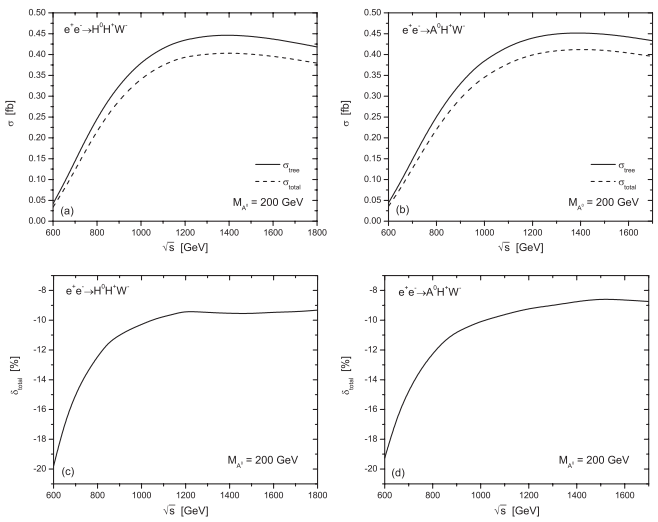

FIG. 7. The Born and full $\mathcal{O}(\alpha_{\rm ew})$ electroweak corrected cross sections as well as the corresponding relative corrections $\delta_{\rm total}$ as the functions of the c.m.s energy $\sqrt{s}$ with $M_{A^0} = 200$ GeV and relevant SPS1a′ MSSM parameters except Higgs sector for processes $e^+e^- \to H^0(A^0)H^+W^-$. (a) cross section versus $\sqrt{s}$ for $e^+e^- \to H^0H^+W^-$, (b) cross section versus $\sqrt{s}$ for $e^+e^- \to A^0H^+W^-$, (c) $\delta_{\rm total}$ versus $\sqrt{s}$ for $e^+e^- \to H^0H^+W^-$, (d) $\delta_{\rm total}$ versus $\sqrt{s}$ for $e^+e^- \to A^0H^+W^-$.

as taken in Figs. 6(a) and 6(b). There we see that when the colliding energy $\sqrt{s}$ goes up, both curves in Figs. 6(c) and 6(d) for relative correction $\delta_{\rm total}$ increase rapidly in the vicinity of threshold energy, and then becomes increasing smoothly with $\delta_{\rm total}$ value being in the range of $[-16\%, -23\%]$ when c.m.s energy is beyond 1.2 TeV.

The Born and full $\mathcal{O}(\alpha_{\rm ew})$ corrected cross sections as the functions of c.m.s energy $\sqrt{s}$ with $M_{A^0} = 200$ GeV and relevant SPS1a′ MSSM parameters except Higgs sector for processes $e^+e^- \to H^0H^+W^-$ and $e^+e^- \to A^0H^+W^-$ are plotted in Figs. 7(a) and 7(b), separately. Again, the values of other Higgs boson masses are obtained from runningthe FormCalc program with input parameter values of $M_{A^0} =$ 200 GeV and OS $\tan\beta = 10.31$. Both the Born cross section and the corrected section increase gently when $\sqrt{s}$ goes beyond the threshold, while when $\sqrt{s}$ approaches 1.2 TeV, the $\mathcal{O}(\alpha_{\rm ew})$ EW corrected cross section can achieve the maximal value of about 0.4 fb. The corresponding EW relative corrections with the same conditions as in Figs. 7(a) and 7(b), are described in Figs. 7(c) and 7(d), respectively. As we can see in these figures, the line-shapes of Born and EW corrected cross sections (relative correction) for $e^+e^- \to H^0H^+W^-$ process are very similar with the corresponding ones for $e^+e^- \to A^0H^+W^-$ process.

The Born and EW corrected cross sections as the functions of input parameter M_{A^0} are drawn in Fig. 8(a) for process $e^+e^- \to H^0H^+W^-$, and the corresponding relative corrections versus M_{A^0} are depicted in Fig. 8(b), with c.m.s energy $\sqrt{s} = 1200$ GeV and the relative MSSM parameters taken from SPS1a′ point except the Higgs sector being fixed by using FormCalc program. In

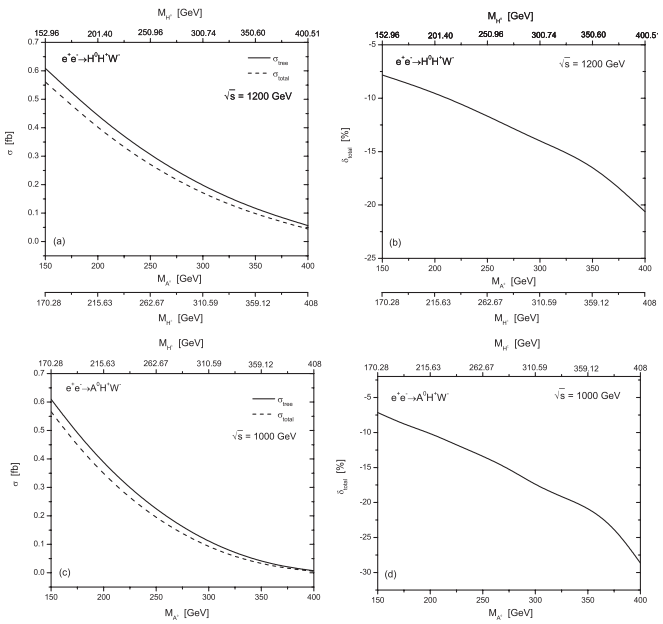

FIG. 8. The Born and full $\mathcal{O}(\alpha_{\rm ew})$ electroweak corrected cross sections as well as the corresponding relative corrections $\delta_{\rm total}$ as the functions of M_{A^0} with c.m.s energy $\sqrt{s} = 1200$ GeV and relevant MSSM parameters in SPS1a′ except Higgs sector, for processes $e^+e^- \to H^0(A^0)H^+W^-$. (a) cross section versus M_{A^0} for $e^+e^- \to H^0H^+W^-$, (b) $\delta_{\rm total}$ versus M_{A^0} for $e^+e^- \to H^0H^+W^-$, (c) cross section versus M_{A^0} for $e^+e^- \to A^0H^+W^-$, (d) $\delta_{\rm total}$ versus M_{A^0} for $e^+e^- \to A^0H^+W^-$.

Fig. 8(a) the one-loop electroweak corrected cross section decreases from 0.56 fb to 0.51 fb with the increment of $M_{H^+}(M_{H^0})$ from 170.28 GeV (152.96 GeV) to 408 GeV (400.51 GeV) for process $e^+e^- \to H^0H^+W^-$. Figure 8(b) shows the relative correction for process $e^+e^- \to H^0H^+W^-$ goes from -7.8% to -20.6% when $M_{H^+}(M_{H^0})$ goes up from 170.28 GeV (152.96 GeV) to 408 GeV (400.51 GeV). For channel $e^+e^- \to A^0H^+W^-$, the cross section and EW relative correction versus M_{A^0} are depicted in Figs. 8(c) and 8(d) respectively, with $\sqrt{s}$ being 1000 GeV and other MSSM parameters taken from SPS1a′ point except Higgs sector being determined by using FormCalc package. We can read from Figs. 8(c) and 8(d) that the EW corrected cross section goes down from 0.56 fb to 0.005 fb and the relative correction varies from -7% to -28.6%, when the input value of M_{A^0} increases from 150 GeV to 400 GeV. In these four parts of Fig. 8, we can see the behavior of these two processes $e^+e^- \to H^0(A^0)H^+W^-$ are very similar except for a tiny difference in the numerical value.

From above numerical results we can see that the experimental statistic errors for processes $e^+e^- \to h^0H^+W^-$, $e^+e^- \to H^0H^+W^-$ and $e^+e^- \to A^0H^+W^-$ can reach 5.5%, 4.2% and 4.2%, respectively. If we assume $\sqrt{s} = 0.6$–1.8 TeV, $\int Ldt \sim 1000$ fb^{-1}, and do not consider the backgrounds to the $e^+e^- \to \Phi^0H^+W^-(\Phi = h^0, H^0, A^0)$ signals and the systematic errors of the experiment (due to lacking their studies at ILC), the EW corrections to the cross sections of these three processes should be taken into account at a linear collider with realistic accuracy better than 10%.

IV. SUMMARY

In this paper, we present the calculation of the full $\mathcal{O}(\alpha_{\rm ew})$ electroweak corrections to the processes $e^+e^- \to \Phi^0H^\pm W^\mp(\Phi = h^0, H^0, A^0)$ at a LC in the MSSM. In the numerical calculation, we generally adopt the MSSM parameters at the reference point SPS1a′ defined in the SPA project. For channel $e^+e^- \to h^0H^\pm W^\mp$, we present the details for treating the charged Higgs boson resonance in the calculation up to one-loop level. Our numerical results show that the EW relative correction for the process $e^+e^- \to h^0H^\pm W^\mp$ can be either positive or negative with the increment of Higgs boson mass M_{A^0}, and the relative correction varies in the range of $[-15\%, 20\%]$ as the M_{A^0} goes from 150 GeV to 400 GeV. For channels $e^+e^- \to H^0(A^0)H^\pm W^\mp$, the EW correction generally reduces the Born cross sections and the relative correction is typically of order $-10\% \sim -20\%$. We conclude that the complete $\mathcal{O}(\alpha_{\rm ew})$ electroweak corrections to the process $e^+e^- \to \Phi^0H^\pm W^\mp(\Phi = h^0, H^0, A^0)$ are generally significant and cannot be neglected in the precise experiment analysis.

ACKNOWLEDGMENTS

This work was supported in part by the National Natural Science Foundation of China, the Education Ministry of China and a special fund sponsored by Chinese Academy of Sciences.

[1] S. L. Glashow, Nucl. Phys. **22**, 579 (1961); S. Weinberg, Phys. Rev. Lett. **19**, 1264 (1967); A. Salam, in *Proceedings of the 8th Nobel Symposium, Stockholm, 1968*, edited by N. Svartholm (Almquist and Wiksells, Stockholm, 1968), p. 367; H. D. Politzer, Phys. Rep. **14**, 129 (1974).

[2] P. W. Higgs, Phys. Lett. **12**, 132 (1964); Phys. Rev. Lett. **13**, 508 (1964); Phys. Rev. **145**, 1156 (1966); F. Englert and R. Brout, Phys. Rev. Lett. **13**, 321 (1964); G. S. Guralnik, C. R. Hagen, and T. W. B. Kibble, *ibid.* **13**, 585 (1964); T. W. B. Kibble, Phys. Rev. **155**, 1554 (1967).

[3] H. P. Nilles, Phys. Rep. **110**, 1 (1984); R. Barbieri, Riv. Nuovo Cimento **11**, 1 (1988).

[4] H. E. Haber and G. L. Kane, Phys. Rep. **117**, 75 (1985).

[5] A. B. Lahanas and D. V. Nanopoulos, Phys. Rep. **145**, 1 (1987).

[6] S. Dawson and M. Oreglia, Annu. Rev. Nucl. Part. Sci. **54**, 269 (2004).

[7] J. A. Aguilar-Saavedra *et al.* (ECFA/DESY LC Physics Working Group Collaboration), hep-ph/0106315; T. Abe *et al.* (American Linear Collider Working Group Collaboration), hep-ex/0106056; K. Abe *et al.* (ACFA Linear Collider Working Group Collaboration), hep-ph/0109166.

[8] S. Komamiya, Phys. Rev. D **38**, 2158 (1988); M. Beccaria, F. M. Renard, S. Trimarchi, and C. Verzegnassi, Phys. Rev. D **68**, 035014 (2003); M. Beccaria, H. Eberl, F. M. Renard, and C. Verzegnassi, Phys. Rev. D **69**, 091301 (2004).

[9] M. Carena and P. M. Zerwas, Report No. CERN 96-01 (unpublished).

[10] P. Janot, Orsay Report No. LAL 91-61, 1991 (unpublished); J.-F. Grivas, Orsay Report No. LAL 91-63, 1991 (unpublished); A. Brignole, J. Ellis, J. F. Gunion, M. Guzzo, F. Olnes, G. Ridolfi, L. Roszkowski, and F. Zwirner (Munich, Annecy, Hamburg Workshop), Report Nos. DESY 92-123A, DESY 92- 123B, DESY 93-123C, edited by P. Zerwas, p. 613 (unpublished); A. Djouadi, J. Kalinowski, and P. M. Zerwas, Z. Phys. C **57**, 569 (1993); P. Janot, in *Proceedings of the 2nd International Workshop on Physics and Experiments with Linear e^+e^- Colliders, Waikoloa, HI, 1993*, edited by F. Harris, S. Olsen, S. Pakvasa, and X. Tata (World Scientific Publishing, Singapore, 1993), p. 192; Report Nos. BNL 52-502, FNAL-PUB -96/112, LBNL-PUB-5425, SLAC Report

No. 485, UCRL-JD-124160 (unpublished); J. F. Gunion, Report No. UCD-97-13, 1997 (unpublished);
[11] A. Sopczak, Z. Phys. C **65**, 449 (1995); Phys. Atom. Nucl. **61**, 938 (1998); Yad. Fiz. **61**, 1030 (1998); Report No. IEKP-KA/97-14 (unpublished).
[12] S. Moretti and W. J. Stirling, Phys. Lett. B **347**, 291 (1995); **366** 451(E) (1996).
[13] E. Accomando *et al.* (ECFA/DESY LC Physics Working Group), Report No. DESY 97-100 [Phys. Rep. 299, 1 (1998)]; A. Djouadi, Report No. LPT-04-133 [Czech. J. Phys. B 55, 23 (2005)]; A. Djouadi, Report No. LPT-Orsay-05-18 (unpublished).
[14] S. Moretti and K. Odagiri, Eur. Phys. J. C **1** 633 (1998).
[15] S. Kanemura, S. Moretti, and K. Odagiri, Report No. CERN-TH/2000-347, KEK-TH-729, MSUHEP-00911, RAL-TR-2000-037 [J. High Energy Phys. issue 02 (2001) 011].
[16] J. Guasch, W. Hollik, and J. Sola, J. High Energy Phys. 10 (2002) 040; W. Hollik, E. Kraus, M. Roth, C. Rupp, K. Sibold, and D. Stoecklinger, Nucl. Phys. **B639**, 3 (2002).
[17] G. Passarino and M. Veltman, Nucl. Phys. **B160**, 151 (1979).
[18] T. Hahn, Comput. Phys. Commun. **140**, 418 (2001).
[19] J. A. M. Vermaseren, math-ph/0010025.
[20] G. J. van Oldenborgh, Comput. Phys. Commun. **66**, 1 (1991).
[21] Y. You, W.-G. Ma, H. Chen, R.-Y. Zhang, Y.-B. Sun, and H.-S. Hou, Phys. Lett. B **571**, 85 (2003); R.-Y. Zhang, W.-G. Ma, H. Chen, Y.-B. Sun, and H.-S. Hou, Phys. Lett. B **578**, 349 (2004).
[22] A. Denner and S. Dittmaier, Nucl. Phys. **B658**, 175 (2003).
[23] S. Eidelman *et al.*, Phys. Lett. B **592**, 1 (2004).
[24] D. Pierce and A. Papadopoulos, Phys. Rev. D **47**, 222 (1993).
[25] R.-Y. Zhang, W.-G. Ma, L.-H. Wan, and Y. Jiang, Phys. Rev. D **65**, 075018 (2002).
[26] J.-J. Liu, W.-G Ma, L. Han, R.-Y. Zhang, Y. Jiang, and P. Wu, Phys. Rev. D **72**, 033010 (2005).
[27] A. Denner, S. Dittmaier, M. Roth, and M. M. Weber, Nucl. Phys. **B660**, 289 (2003).
[28] A. Djouadi, J. Kalinowski, and M. Spira, Comput. Phys. Commun. **108**, 56 (1998).
[29] B. W. Harris and J. F. Owens, Phys. Rev. D **65**, 094032 (2002).
[30] G. 't Hooft and M. Veltman, Nucl. Phys. **B153**, 365 (1979).
[31] A. Denner, Fortschr. Phys. **41**, 307 (1993).
[32] T. Ishikawa, T. Kaneko, K. Kato, S. Kawabata, Y. Shimizu, and H. Tanaka, KEK Report No. 92-19, 1993 (unpublished).
[33] F. Jegerlehner, Report No. DESY 01-029 (unpublished).
[34] J. A. Aguilar-Saavedra *et al.*, Eur. Phys. J. C **46**, 43 (2006).
[35] B. C. Allanach *et al.*, in *Proc. of the APS/DPF/DPB Summer Study on the Future of Particle Physics (Snowmass 2001)*, edited by N. Graf, eConf C010630, P125 (2001) [Eur. Phys. J. C 25, 113 (2002)].
[36] Thomas Hahn and Christian Schappacher, Comput. Phys. Commun. **143**, 54 (2002).